International Journal of Fluid Machinery and Systems
Vol. 2, No. 2, April-June 2009

Original Paper

Dynamic Characteristics of the Radial Clearance Flow between Axially Oscillating Rotational Disk and Stationary Disk

Hironori Horiguchi[1], Yoshinori Ueno[1], Koutaro Takahashi [2]
Kazuyoshi Miyagawa[3] and Yoshinobu Tsujimoto[1]

[1]Graduate School of Engineering Science, Osaka University
1-3 Machikaneyama, Toyonaka, Osaka, 560-8531, Japan
[2]School of Engineering Science, Osaka University
1-3 Machikaneyama, Toyonaka, Osaka, 560-8531, Japan
[3]Takasago Research and Development Center
Mitsubishi Heavy Industries, Ltd.
2-1-1 Shinhama, Arai-cho, Takasago, Hyogo, 676-8686, Japan

Abstract

Dynamic characteristics of the clearance flow between an axially oscillating rotational disk and a stationary disk were examined by experiments and computations based on a bulk flow model. In the case without pressure fluctuations at the inlet and outlet of the clearance, parallel and contracting flow paths had an effect to stabilize the axial oscillation of the rotating disk. The enlarged flow path had an effect to destabilize the axial oscillation due to the negative damping and stiffness for outward and inward flows, respectively. It was shown that the fluid force can be decomposed into the component caused by the inlet or outlet pressure fluctuation without the axial oscillation and that due to the axial oscillation without the inlet or outlet pressure fluctuation. A method to predict the stiffness and damping coefficients is proposed for general cases when the device is combined with an arbitrary flow system.

Keywords: Pump, Flow Induced Vibration, Axisymmetric Flow, Clearance Flow, Balance Disk, Bulk Flow Model

1. Introduction

Thrust bearings are used to compensate the axial thrust on the impeller. When the thrust is excessive, a balance disk or a balance piston is often used to reduce the load of the bearings. For balancing devices, it is important to clarify their dynamic characteristics to avoid self-excited axial oscillation [1].

Dynamic characteristics of the flow in an one-dimensional, narrow, tapered clearance was investigated by Inada, et al. [2]. Childs [3] and Brennen [4] have examined the dynamic characteristics of flows in seals and in the clearance between casing and front shroud of impellers. However, dynamic characteristics of the radial clearance flow between stationary and rotating disk under axial oscillation have not been clarified yet.

In the present study, the dynamic characteristics of the flow between stationary and rotating disks under axial oscillation were studied by experiments and computations based on a bulk flow model.

2. Experimental Facilities and Procedure

Figure 1 shows the cross section of experimental facility. The disk on the left is stationary and the disk on the right rotates with axial oscillation. The rotating disk is supported by the shaft shown on the right side of the disk. The rotating disk is fixed on a bush housing with a keyway and can oscillate in the axial direction. The oscillation is given by the shaft shown on the left side of the disk. Air at room temperature is the working fluid. In the case when a radial outward flow is generated in the clearance between the stationary and rotating disks, the air is supplied into the test section through the two ports shown in the left side of the stationary disk. In order to suppress the occurrence of a swirling flow at the inlet of the clearance, the air is supplied radially and two ports are placed at an angular distance of 180 degrees. For the case with inward flow, the air is discharged through the ports.

Received April 1 2009; accepted for publication May 15 2009: Review conducted by Prof. Wang Le-qing. (Paper number O09007)
Corresponding author: Hironori Horiguchi, Associate Professor, horiguti@me.es.osaka-u.ac.jp

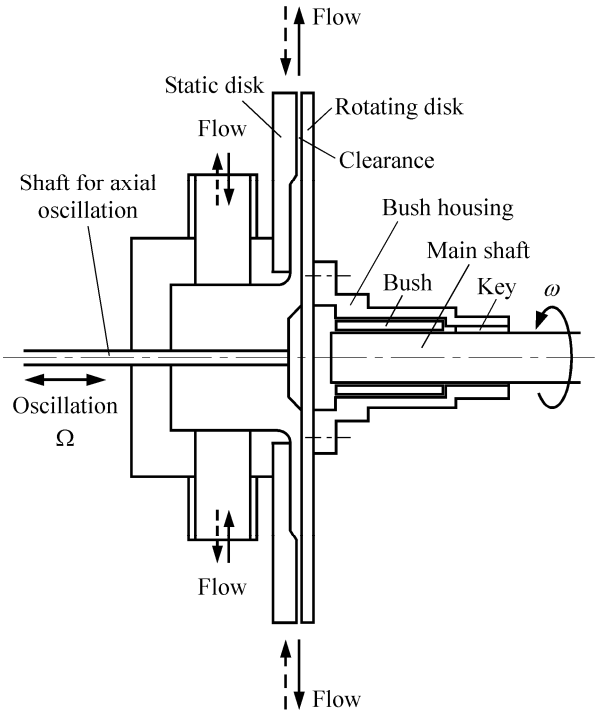

Fig. 1 Cross section of the test section

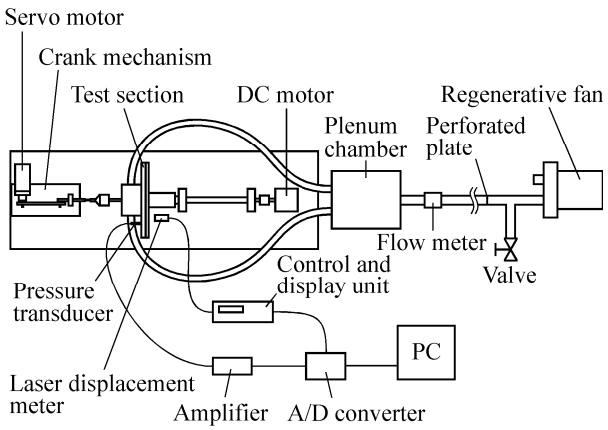

Fig. 2 Front view of the experimental setup

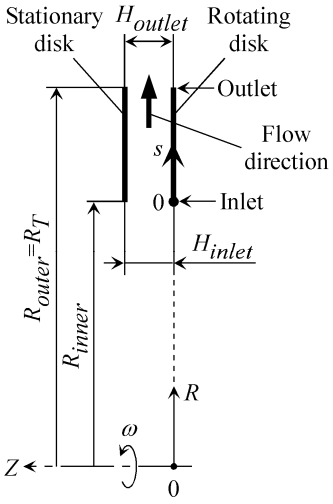

Fig. 3 Coordinates and parameters of the clearance

Table 1 Geometry of the clearance

	Parallel flow path	Enlarged flow path	Contracting flow path
H_{inlet} [mm]	1.0	0.5	1.0
H_{outlet} [mm]	1.0	1.0	0.5

A schematic layout of the experimental facility is shown in Fig.2. The air as the working fluid is supplied by the regenerative fan shown in the right side of Fig.2 through the perforated plate, the flow meter (Nagano Keiki, NV91), and the plenum chamber. In the regenerative fan, the temperature of the discharged air increases largely at low flow rates. Therefore, the fan was operated at high flow rates and the flow rate through the test section was controlled by discharging excessive air through the valve. In the case with inward flow, the suction port of the fan was connected to the pipe. The axial oscillation of the rotating disk was given by the crank mechanism from the left hand side of the facility through a bearing.

Fluctuating pressure in the clearance was measured by semiconductor pressure transducers (JTEKT PD-104KW) flash mounted on the stationary disk. The flow direction at the inlet of the clearance was measured by an one hole pitot tube. An axial displacement of the rotating disk was measured by a displacement sensor (KEYENCE LC-2450). The signal from the pressure transducer was amplified by an amplifier (JTEKT AA6010) and recorded in a computer using the software (ELMEC WAAP-WIN Ver.4.7) through the A/D converter (ELMEC EC-2371A) as well as the signal from the displacement sensor. FFT analysis was made on the pressure signal. The amplitude and the phase of the pressure fluctuation at the frequency of axial oscillation are determined relative to the clearance fluctuation of $\bar{H}_1 e^{j\Omega t}$. The amplitude of the axial oscillation of the rotating disk was set to be about 0.2mm.

The dynamic characteristics were measured for three types of clearance flow; parallel, enlarged and contracting. The inlet and outlet widths of the clearance are shown in Fig.3. The inner and outer radii are, $R_{inner} = 70\text{mm}$ and $R_{outer} = 100\text{mm}$. The normalized coordinate $s(= S / L_s)$ along the meridional stream line on the rotating disk is equal to 0 and 1 at the inlet and outlet of the clearance, respectively. The widths H_{inlet} and H_{outlet} of the clearance at the inlet and outlet of each clearance were shown in Table 1. The rotational frequency $2\pi\omega$ of the rotating disk is 20Hz (1200rpm).

The experiment and the computation were also carried out in the case of the inward clearance flow. The inlet and outlet widths H_{inlet} and H_{outlet} of the clearances at the inlet and outlet are the same as those shown in Table 1.

In the present study, the amplitude of the pressure fluctuation is quite small. Therefore, the calibration tests of the pressure transducers were done. The uncertainty of them was $\pm 3\%$.

Table 2 Loss and discharge coefficients in the outward flow

	Loss coefficient, ξ	Discharge coefficient, C_{de}
Parallel flow path	0.15	0.92
Enlarged flow path	0.23	0.89
Contracting flow path	0.92	0.84

Table 3 Loss and discharge coefficients in the inward flow

	Loss coefficient, ξ	Discharge coefficient, C_{de}
Parallel flow path	0.05	1.0
Enlarged flow path	0.14	0.97
Contracting flow path	0	0.95

3. Computation

3.1 Model of Computation

For the computation, the bulk flow model [3] is used, which assumes uniform velocity and pressure distributions over the clearance considering the wall shear and the oscillation of the clearance width.

Governing equations are a continuity equation and momentum equations in the meridional and circumferential directions. The turbulent lubrication model presented by Hirs [5] is used as the wall shear stress.

The width of the clearance, the velocity and the pressure are divided into steady and unsteady components due to the axial oscillation with the frequency Ω. The unsteady components are assumed to be much smaller than the steady components. Based on this assumption, the governing equations are linearized.

3.2 Computation of the Clearance Flow

After the linearization of the governing equations, the equations of steady and unsteady components are obtained. By solving the equation of the steady components using boundary conditions, a steady flow field is determined. By solving the equations of the unsteady components using boundary conditions and the steady velocity and pressure distributions, the unsteady flow field is obtained.

3.3 Boundary Conditions for Outward Flow

In the case of outward flow, the pressure $P(0)$ just after the inlet into the clearance and the pressure $P(1)$ just before the outlet from the clearance are expressed as follows.

$$P(0) = P_{inner} - \frac{\rho}{2}(1+\xi)U_s^2(0)$$
$$P(1) = P_{outer} + \frac{\rho}{2}(C_{de}-1)[U_s^2(1)+U_\theta^2(1)] \quad (1)$$

where ξ is a loss coefficient at the inlet of the clearance and C_{de} is a discharge coefficient at the outlet of the clearance. To determine the value of ξ, the pressure at R =64mm before the inlet of the clearance was measured and the Bernoulli's equation was applied between R =64mm and R =70mm for estimating the pressure P_{inner} at R =70mm just before the inlet of the clearance. To determine the value of C_{de}, the pressure P_{outer} just after the outlet of the clearance was assumed to equal the atmospheric pressure P_{air}.

By measuring the flow direction at the inlet of the clearance by the pitot tube, it was found that the circumferential velocity at the inlet of the clearance was nearly equal to 0. Therefore, the steady circumferential velocity $U_{\theta 0}(0)$ at the inlet of the clearance was assumed to be 0. The steady meridional velocity $U_{s0}(0)$ at the inlet of the clearance was given, depending on the flow rate. The unsteady components of the velocity just after the outlet of the clearance were assumed to be 0.

The values of the loss coefficient ξ and the discharge coefficient C_{de} were determined so that pressure distributions obtained by the computation of the steady flow agrees with those in the experiment without the axial oscillation of the rotating disk. The values of ξ and C_{de} are shown in Table 2.

3.4 Boundary Conditions for Inward Flow

In the case of inward flow, the following boundary conditions are used.

$$P(0) = P_{outer} - \frac{\rho}{2}(1+\xi)U_s^2(0)$$
$$P(1) = P_{inner} + \frac{\rho}{2}(C_{de}-1)[U_s^2(1)+U_\theta^2(1)] \quad (2)$$

The pressure P_{outer} just before the inlet of the clearance is assumed to equal the atmospheric pressure P_{air}. The pressure at R =64mm downstream from the outlet of the clearance was measured and the pressure P_{inner} at R =70mm just after the outlet of the clearance was estimated by the Bernoulli's equation. The steady circumferential velocity $U_{\theta 0}(0)$ at the inlet of the clearance was assumed to be 0. The steady meridional velocity $U_{s0}(0)$ at the inlet of the clearance was given, depending on the flow rate. The unsteady components of the velocity just before the inlet of the clearance were assumed to be 0. The values of ξ and C_{de} used in the computation are shown in Table 3.

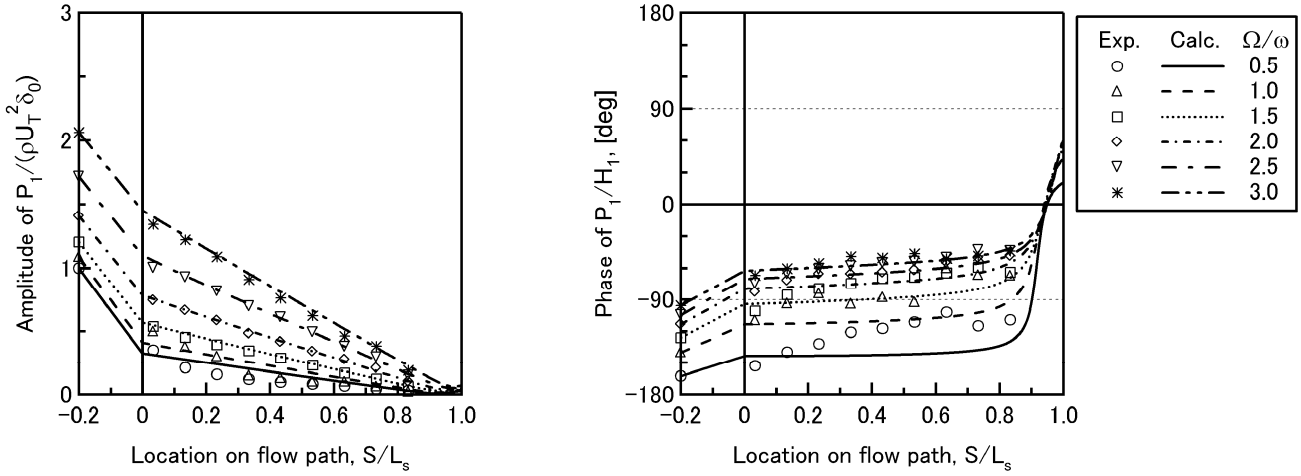

(a) Amplitude (b) Phase

Fig. 4 Amplitude and phase of the pressure in the outward flow through the parallel flow path at ϕ=0.63

3.5 Stiffness and Damping Coefficients

The fluid force F on the rotating disk is expressed as follows, using a stiffness coefficient K and a damping coefficient C.

$$F = -KZ - C\dot{Z} \tag{3}$$

where

$$F = \bar{F}_1 e^{j\Omega t}$$

$$Z = \bar{Z} e^{j\Omega t} = -\bar{H}_1 e^{j\Omega t} = -\delta_0 H_i e^{j\Omega t}$$

Dividing Eq.(3) by $\pi R_T^2 \rho U_T^2$, the nondimensional fluid force $\bar{f}_1 = \bar{F}_1 / (\pi R_T^2 \rho U_T^2)$ is defined as follow.

$$\frac{\bar{f}_1}{\delta_0} = \frac{KH_i}{\pi R_T^2 \rho U_T^2} + j\frac{\Omega C H_i}{\pi R_T^2 \rho U_T^2} \tag{4}$$

It is found from Eq.(4) that the stiffness coefficient K and the damping coefficient C are proportional to the real and imaginary parts of the complex amplitude $\bar{f}_1$ of the nondimensional unsteady fluid force f_1, respectively. When the real and imaginary parts of the complex amplitude $\bar{f}_1$ are negative, the values of K and C are also negative. If we represent $\bar{f}_1 = |\bar{f}_1| e^{j\theta}$, the value of K is negative if $-180\,\mathrm{deg} \le \theta < -90\,\mathrm{deg}$ or $90\,\mathrm{deg} < \theta \le 180\,\mathrm{deg}$ where the real part of $\bar{f}_1$ is negative. The value of C is negative if $-180\,\mathrm{deg} < \theta < 0\,\mathrm{deg}$ where the imaginary part of $\bar{f}_1$ is negative. If we represent the pressure fluctuation $\bar{P}_1 = |\bar{P}_1| e^{j\theta}$, it contributes to negative K if $-90\,\mathrm{deg} < \theta < 90\,\mathrm{deg}$ and to negative C if $0\,\mathrm{deg} < \theta < 180\,\mathrm{deg}$.

4. Results and Discussions

4.1 Unsteady Pressure Distribution

The amplitude and phase of the fluctuating pressure $\bar{P}_1 e^{j\Omega t}$ for the oscillating width $\bar{H}_1 e^{j\Omega t}$ of the clearance for outward flow in the parallel flow path is shown in Fig.4. The experimental and numerical results at the flow rate $\phi = 0.63$ ($Q = 0.005\mathrm{m}^3/\mathrm{s}$) are shown. $S = 0$ corresponds to the inlet at inner radius. Ω and ω are the angular frequency of the axial oscillation of the rotating disk and the rotational angular frequency, respectively.

The experimental and numerical results are a little different at low frequency ratios $\Omega/\omega = 0.5$ and 1.0, but at other frequency ratios these results are similar. The experiment and computation for the enlarged and contracting flow paths were also conducted and those results agreed qualitatively with the results of the parallel flow path shown in Fig.4. This shows the validity of the bulk flow model.

It is found in Fig.4 that the amplitude of the pressure fluctuation increases as the frequency ratio increases. If the frequency ratio is larger than 2.0, the phases θ at almost all of measuring points have the values between $-90\,\mathrm{deg}$ and $90\,\mathrm{deg}$. This contributes to make *K* to be negative.

The amplitude and phase of the fluctuating pressure for the inward flow through the parallel flow path at $\phi = 0.63$ is shown in Fig.5. $S = 0$ corresponds to the inlet at outer radius. The numerical results agree with the experimental results well. It is found that the amplitude of the pressure fluctuation increases as the frequency ratio increases. The phases θ of the pressure fluctuation are between $-90\,\mathrm{deg}$ and $90\,\mathrm{deg}$. This means that the values of *K* are negative.

In the outward flow, the phase θ of the pressure fluctuation is quasi-statically $-180\,\mathrm{deg}$ and increases (proceeds) as the frequency ratio increases. On the other hand, in the inward flow, the phase θ is quasi-statically $0\,\mathrm{deg}$ and decreases (delays) as the frequency ratio increases.

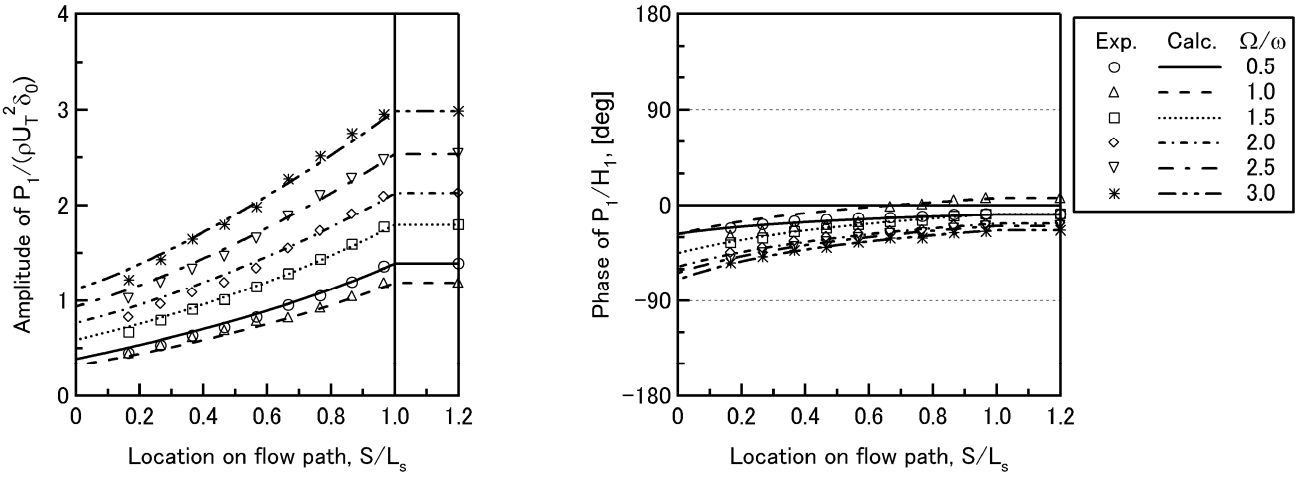

(a) Amplitude (b) Phase

Fig. 5 Amplitude and phase of the pressure in the inward flow through the parallel flow path at ϕ=0.63

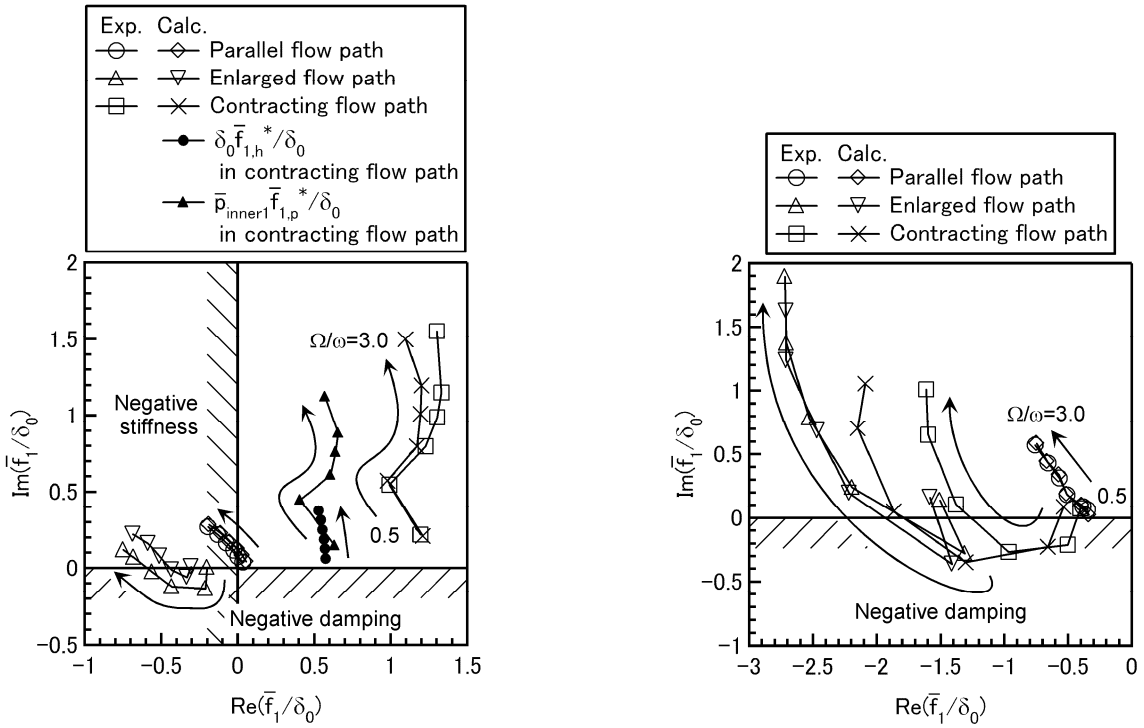

(a) Outward flow (b) Inward flow

Fig. 6 Real and imaginary parts of the normalized fluid force $\bar{f}_1/\delta_0$ at ϕ=0.63

4.2 Unsteady Fluid Forces

By integrating the pressure distributions shown in Figs.4 and 5, the unsteady fluid force on the rotating disk was estimated. The values of the nondimensional fluid forces $\bar{f}_1/\delta_0$ defined in Eq.(4) are shown in Figs.6(a) and (b) for the outward and inward flows, respectively. The horizontal axes in Fig.6 are the real part of $\bar{f}_1/\delta_0$ and represent the nondimensional stiffness. The vertical axes are the imaginary part of $\bar{f}_1/\delta_0$ and represent the nondimensional damping. The results are for the frequencies from 0.5 to 3.0 at 0.5 intervals.

In the outward flow in the parallel flow path, as shown in Fig.6(a), the damping coefficients are positive, but the stiffness coefficients are negative when the frequency ratio is larger than 1.0. In the enlarged flow path, the damping coefficients are positive except the case of the smaller frequency ratios, but the stiffness coefficients are negative in all frequency ratios. In the contracting flow path, both of the damping and stiffness coefficients are positive. In the case of the inward flow, as shown in Fig.6(b), the stiffness coefficients are negative in all flow paths. The amplitudes of the fluid forces are larger in the outward flow passed through the contracting flow path and in the inward flow passed through the enlarged flow path, where the minimum widths of the clearance are at the periphery of the rotating disk.

In the present paper, only the results at $\phi = 0.63$ are shown. The experiment and computation were conducted for the cases of the low flow rate $\phi = 0.25$ ($Q = 0.002\ \mathrm{m}^3/\mathrm{s}$) and the high flow rate $\phi = 1.27$ ($Q = 0.01\ \mathrm{m}^3/\mathrm{s}$). As the flow rate increased,

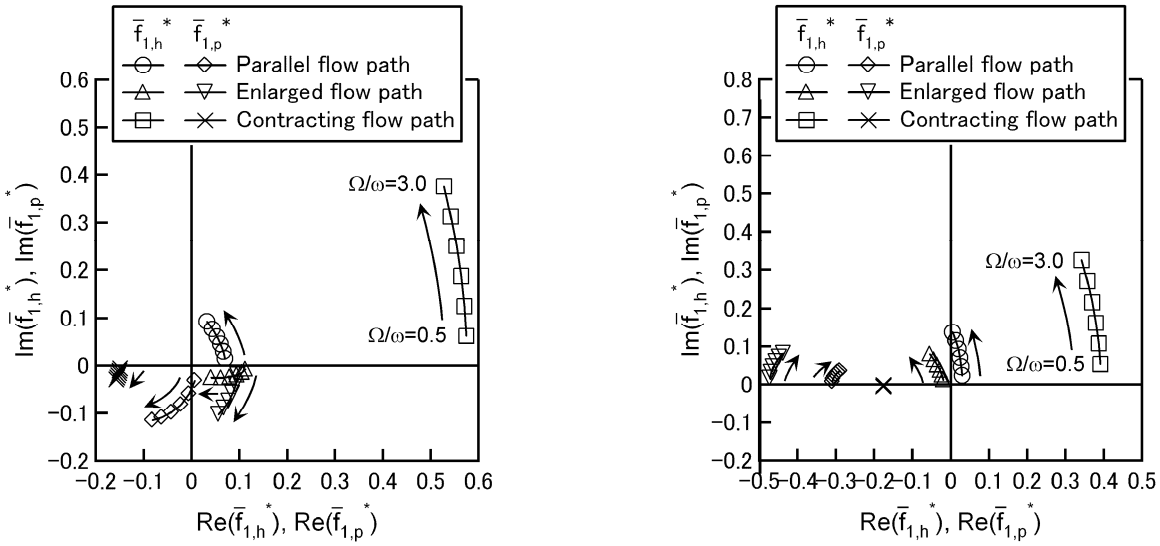

Fig. 7 Real and imaginary parts of the computational normalized fluid forces $\bar{f}_{1,h}^{*}$ and $\bar{f}_{1,p}^{*}$ at ϕ=0.63

the amplitudes of the pressure fluctuation and fluid force $\bar{f}_1 / \delta_0$ increased. However, these results are qualitatively the same as the results at $\phi = 0.63$.

In the results of the present study, the contracting flow path where the fluid flows radially outward seems to be appropriate for a balance disk. The fluid force largely depends on the larger pressure fluctuation at the inner radius of the clearance, as shown in Figs.4(a) and 5(a). In the computation of the present study, the experimental pressure fluctuation at the inner radius of the clearance was used. However, it needs to be predicted for general cases.

In the next section, the dynamic characteristics of the clearance flow are discussed.

4.3 Decomposition of the Dynamic Characteristics of the Clearance Flow

When the width of the clearance oscillates, the flow rate fluctuation occurs. The pressure fluctuation at the inner radius and the fluctuation of the fluid force are determined, as a result of the response of other components connected with the system to the flow rate fluctuation. In the present study, as the small disturbance of the flow is assumed, the fluctuating flow rate and fluid force can be decomposed into (I) the fluctuating flow rate $\bar{q}_{1,h}^{*} e^{j\Omega t}$ at the inner radius of the clearance and the fluctuating fluid force $\bar{f}_{1,h}^{*} e^{j\Omega t}$ due to the oscillation of the clearance width $\delta_0 e^{j\Omega t}$ without the pressure fluctuation at the inner radius of the clearance, and (II) the fluctuating flow rate $\bar{q}_{1,p}^{*} e^{j\Omega t}$ at the inner radius of the clearance and the fluctuating fluid force $\bar{f}_{1,p}^{*} e^{j\Omega t}$ due to the fluctuating pressure $\bar{p}_{inner1} e^{j\Omega t}$ at the inner radius of the clearance without the oscillation of the clearance width. $\bar{f}_{1,h}^{*}$ and $\bar{f}_{1,p}^{*}$ are the nondimensional fluid forces, $\bar{q}_{1,h}^{*}$ and $\bar{q}_{1,p}^{*}$ are the nondimensional flow rates at $R = R_{inner} = 70\mathrm{mm}$. There values are defined as follows.

$$f_{1,h} = \bar{f}_{1,h} e^{j\Omega t} = \delta_0 \bar{f}_{1,h}^{*} e^{j\Omega t}, \quad \bar{f}_{1,h}^{*} = \frac{\bar{f}_{1,h}}{\delta_0}$$

$$q_{1,h} = \bar{q}_{1,h} e^{j\Omega t} = \delta_0 \bar{q}_{1,h}^{*} e^{j\Omega t}, \quad \bar{q}_{1,h}^{*} = \frac{\bar{q}_{1,h}}{\delta_0}$$

$$f_{1,p} = \bar{f}_{1,p} e^{j\Omega t} = \bar{p}_{inner1} \bar{f}_{1,p}^{*} e^{j\Omega t}, \quad \bar{f}_{1,p}^{*} = \frac{\bar{f}_{1,p}}{\bar{p}_{inner1}}$$

$$q_{1,p} = \bar{q}_{1,p} e^{j\Omega t} = \bar{p}_{inner1} \bar{q}_{1,p}^{*} e^{j\Omega t}, \quad \bar{q}_{1,p}^{*} \equiv \frac{\bar{q}_{1,p}}{\bar{p}_{inner1}}$$

When the pressure fluctuation at the inner radius of the clearance and the oscillation of the clearance width occur together, the following equations can be given.

$$\begin{aligned} f_1 &= \delta_0 \bar{f}_{1,h}^{*} e^{j\Omega t} + \bar{p}_{inner1} \bar{f}_{1,p}^{*} e^{j\Omega t} \\ q_1 &= \delta_0 \bar{q}_{1,h}^{*} e^{j\Omega t} + \bar{p}_{inner1} \bar{q}_{1,p}^{*} e^{j\Omega t} \end{aligned} \tag{5}$$

The numerical results of $\bar{f}_{1,h}^{*}$ and $\bar{f}_{1,p}^{*}$ are shown in Figs.7(a) and (b) for the outward and inward flows, respectively. In Fig.7(a) for the outward flow, the real part of $\bar{f}_{1,h}^{*}$ is positive and the imaginary part of $\bar{f}_{1,h}^{*}$ changes from negative to positive values as the geometry of the flow path changes in the order of the enlarged, parallel and contracting flow paths. The real part of $\bar{f}_{1,p}^{*}$ changes from positive values to negative values and the imaginary part of $\bar{f}_{1,p}^{*}$ remains negative.

In the quasi-steady case that the frequency ratio is 0, the imaginary parts of $\bar{f}_{1,h}^{*}$ and $\bar{f}_{1,p}^{*}$ are 0. The values of $\bar{f}_{1,h}^{*}$ and $\bar{f}_{1,p}^{*}$ depart from the line where the imaginary part is 0 as the frequency ratio increases.

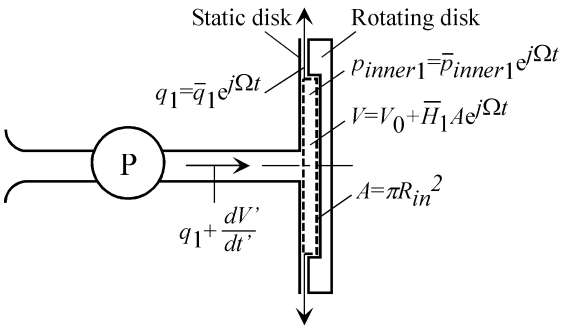

Fig. 8 System of a pump and the clearance

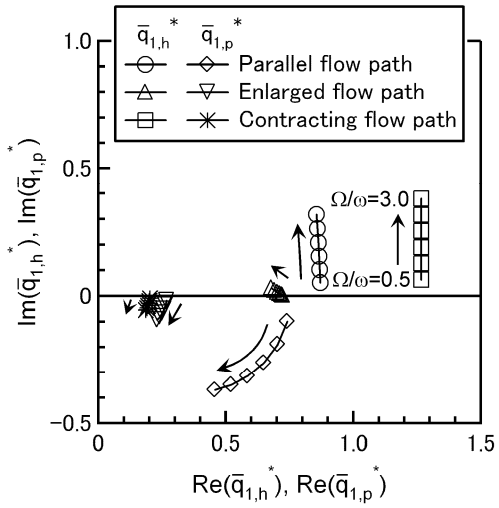

(a) Outward flow

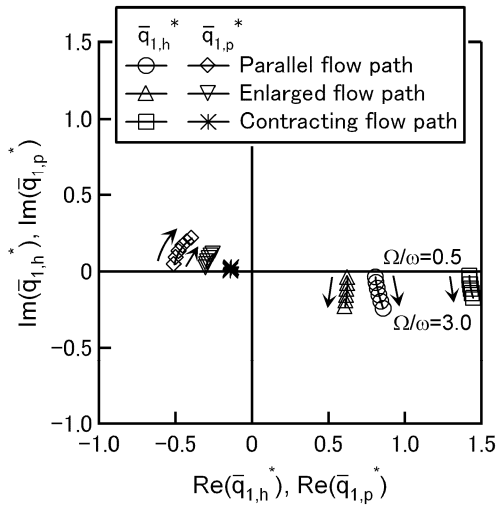

(b) Inward flow

Fig. 9 Real and imaginary parts of the normalized flow rates $\bar{q}_{1,h}^*$ and $\bar{q}_{1,p}^*$ at ϕ=0.63 in the computation

In Fig. 7(b) for the inward flow, as the geometry of the flow path changes in the order of the enlarged, parallel, and contracting flow paths, the real part of $\bar{f}_{1,h}^*$ changes from negative values to positive values but the imaginary part of $\bar{f}_{1,h}^*$ remains positive. The real part of $\bar{f}_{1,p}^*$ is negative and the imaginary part of $\bar{f}_{1,p}^*$ is positive.

The values of δ_0 is smaller than 1 and set about 0.2 in the present study. The magnitude of $\bar{p}_{inner1}$ was about 1□7.5 in the outward flow and about 1□14 in the inward flow. As an example, the values of $\delta_0\bar{f}_{1,h}^*$ and $\bar{p}_{inner1}\bar{f}_{1,p}^*$ divided by δ_0 for the outward flow in the contracting flow path are shown in Fig.6(a). It is found that the sum of these values is equal to the value of $\bar{f}_1/\delta_0$ and the effect of the pressure fluctuation at the inner radius of the clearance is large. In other cases, $\bar{f}_{1,h}^*$ in Figs.7(a) and (b) represents the effect of the oscillation of the clearance width and the difference of $\bar{f}_1/\delta_0$ in Figs.6(a) and (b) from $\bar{f}_{1,h}^*$ in Figs.7(a) and (b) represents the effect of the pressure fluctuation $\bar{p}_{inner1}\bar{f}_{1,p}^*/\delta_0$ at the inner radius of the clearance. As the magnitude of the fluid force $\bar{f}_1/\delta_0$ in Figs.6(a) and (b) are quite larger than that of $\bar{f}_{1,h}^*$ in Figs.7(a) and (b), the effect of the pressure fluctuation at the inner radius is larger in the present experiment. It is found that, in the basic case without the pressure fluctuation at the inner radius, the stiffness and damping coefficients in the parallel and contracting flow paths are positive in the outward and inward flows but in the enlarged flow path the damping coefficient is negative in the outward flow and the stiffness coefficient is negative in the inward flow. The characteristics of $\bar{f}_{1,h}^*$ are similar in the outward and inward flows. So, the effect of the pressure fluctuation ($\bar{p}_{inner1}\bar{f}_{1,p}^*e^{j\Omega t}$) at the inner radius is larger in the inward flow.

Using the results shown in Figs.7(a) and (b), the stiffness and damping coefficients can be estimated for various combinations of $\bar{p}_{inner1}$ and δ_0. In the next section, the prediction method of $\bar{p}_{inner1}$ is discussed.

4.4 Prediction Method of the Pressure Fluctuation at the Inner Radius of the Clearance

The pressure fluctuation at the inner radius is determined from characteristics of the flow rate in the clearance and the flow system. We consider a simple flow system with a pump resistance *R* as shown in Fig.8. It is assumed that the volume of the inside of the inner diameter of the clearance changes but the pressure in it is uniform. The pressure in the inside of the inner diameter of the clearance is expressed with the pump resistance R' and the flow rate q_1 through the clearance as follows.

$$p_{inner1}=-R'\left(q_1+\frac{dV'}{dt'}\right) \tag{6}$$

where V' is the nondimensional volume of the inside of the inner radius of the clearance and defined as follow.

$$V'=\frac{V}{\pi D_T^2 H_i}=V_0'+A'\delta_0 e^{j\Omega' t'}$$
$$\Omega'=\Omega\frac{D_T}{U_T},\quad A'=\frac{A}{\pi D_T^2},\quad R'=\frac{2\pi H_i}{\rho\Omega}R,\quad t'=t\frac{U_T}{D_T} \tag{7}$$

Substituting Eq.(7) and q_1 represented by Eq.(5) into Eq.(6), the following equation can be given.

$$\bar{p}_{inner1} = -\frac{\bar{q}_{1,h}^{\ *} + j\Omega' A'}{1 + R' \cdot \bar{q}_{1,p}^{\ *}} R' \delta_0$$

Using the above equation and the values of $\bar{q}_{1,h}^{\ *}$, $\bar{q}_{1,p}^{\ *}$ and δ_0, the pressure $\bar{p}_{inner1}$ at the inner radius of the clearance is determined. By using the values of $\bar{p}_{inner1}$ and Eq.(5), the fluid force f_1 is estimated. The values of $\bar{q}_{1,h}^{\ *}$ and $\bar{q}_{1,p}^{\ *}$ in the outward and inward flows are shown in Figs.9(a) and (b), respectively.

In the outward flow, the flow rate increases in the steady case without the oscillation of the clearance width as the clearance width and the pressure at the inner radius of the clearance increase. Therefore, the values of $\bar{q}_{1,h}^{\ *}$ and $\bar{q}_{1,p}^{\ *}$ are positive real values at the lower frequency as shown in Fig.9(a). In the inward flow, the flow rate decreases in the steady case as the pressure at the inner radius of the clearance increases. Consequently, the values of $\bar{q}_{1,p}^{\ *}$ are negative real values at the lower frequency as shown in Fig.9(b). As the frequency of the oscillation increases, the phase delays except $\bar{q}_{1,h}^{\ *}$ of the outward flow through the parallel flow path.

In order to predict the values of $\bar{p}_{inner1}$ measured in the present study, various models of the flow system were considered but a suitable model could not be obtained. In the present paper, the simplest model was discussed to demonstrate that the values of $\bar{p}_{inner1}$ can be predicted in principle.

5. Conclusions

The dynamic characteristics of the clearance flow between stationary and rotating/axially oscillating disks were examined in the experiment and the computation based on the bulk flow model. The results can be summarized as follows.

(1) In the case when the pressures at the inlet and outlet of the clearance are constant, the fluid force can suppress the axial oscillation of the disk in the parallel and contracting flow paths. But in the enlarged flow path, the fluid force can enhance the axial oscillation of the disk due to the negative damping coefficient of the clearance flow in the outward flow and the negative stiffness coefficient in the inward flow.

(2) The amplitude of the pressure fluctuation at the inner radius of the clearance was large in the flow system of the present study. If the fluctuating pressure obtained in the experiment were used as boundary conditions, the fluctuating fluid forces could be simulated well by the bulk flow model.

(3) The pressure fluctuation at the inner radius of the clearance is determined from the characteristics of the flow through the clearance and the flow system connected with the clearance. The unsteady characteristics of the flows caused by the oscillation of the width of the flow path, and by the inlet pressure were determined. The results can be used to determine the fluid forces for general cases.

Acknowledgement

The authors would like to thank Takeshi Okubo, Katsuya Yamashita, and Shinji Fukao in Mitsubishi Heavy Industries, Ltd. for their help to carrying out the present study. The authors also thank graduate student Hideyoshi Shibata, and undergraduate student Zigen Tatsukawa for their cooperation of the experiment and the computation.

Nomenclature

A	Area of the circle with the inner diameter of the clearance [m^2]	U_T	Tip speed of the rotating disk [m/s]
C	Damping coefficient of the clearance flow [N/(m/s)]	V	Inner volume from the inside diameter of the clearance [m^3]
C_{de}	Discharge coefficient	δ_0	Nondimensional amplitude of the axial oscillation of the disk $= \bar{H}_1 / H_i$
D_T	Diameter of the rotating disk =200 [mm]	ϕ	Flow coefficient $= Q / (\pi D_T H_i U_T)$
f	Nondimensional fluid force = $F / (\pi R_T^2 \rho U_T^2)$	θ	Phase angle [rad] or [deg]
f^*	Nondimensional fluid force = f / δ_0 or f / p_{inner1}	ρ	Density of the fluid [kg/m^3]
F	Fluid force acting on the rotating disk [N]	ω	Rotational angular frequency of the shaft $= 40\pi$ [rad/s]
H	Width of the clearance between the rotating disk and the stationary disk [m]	Ω	Angular frequency of the axial oscillation [rad/s]
H_i	Characteristic clearance width =1.0 [mm]	ξ	Loss coefficient
j	Imaginary unit	**Superscript**	
K	Stiffness coefficient of the clearance flow [N/m]	$-$	Complex amplitude
L_s	Length of the flow path in the clearance along the meridional stream line [m]	**Subscript**	
		h	Value in the case of $P_{inner1} = 0$
p	Nondimensional pressure = $P / (\rho U_T^2)$	*inlet*	Value at the inlet of the clearance
P	Pressure [Pa]	*inner*	Value at the inner side (R=70[mm]) of the clearance
q	Nondimensional volume flow rate $= Q / (\pi D_T H_i U_T)$	*outlet*	Value at the outlet of the clearance
		outer	Value at the outer side (R=100[mm]) of

Q	Volume flow rate [m^3/s]		the clearance
R	Radial position [m] or pump resistance [Pa/(m^3/s)]	p	Value in the case of $\delta_0 = 0$
		s	Meridional component (Component of s direction)
R_T	Radius of the rotating disk =100 [mm]		
s	Nondimensional coordinate alone the meridional stream line = S / L_s	θ	Circumferential component
		0	Steady component
S	Coordinate alone the meridional stream line [m]	1	Component of small disturbance
		Others	
t	Time [s]	Re(X)	Real part of X
U	Velocity [m/s]	Im(X)	Imaginary part of

References

[1] Makay, E. and Szamody, O., 1978, "Survey of Feed Pump Outages," Final Report of Research Project 641, Electric Power Research Institute, FP-754, pp. 4_10-4_12 and pp. A-35.

[2] Inada, F. and Hayama, S., 1987, "A Study on Leakage-Flow-Induced Vibrations (1st Report, Fluid-Dynamic Forces Acting on the Walls of an One-Dimensional, Narrow, Tapered Passage)," Trans. Jpn. Soc. Mech. Eng., Ser. C, Vol. 53, No. 488, pp. 933-939 (in Japanese).

[3] Childs, D. W., 1991, "Fluid-Structure Interaction Forces at Pump-Impeller-Shroud Surfaces for Axial Vibration Analysis," ASME Trans. J. Vibration and Acoustics, Vol. 113, No. 1, pp. 108-115.

[4] Hsu, Y. and Brennen, C. E., 2002, "Fluid Flow Equations for Rotordynamic Flows in Seals and Leakage Paths," ASME Trans. J. Fluids Eng., Vol. 124, No. 1, pp. 176-181.

[5] Hirs, G. G., 1973, "A Bluk-Flow Theory for Turbulence in Lubricant Film," ASME Trans. J. Lubrication Technology, pp. 137-146.